

Cite this: *Dalton Trans.*, 2022, **51**, 6944

# Growth, structure, and temperature dependent emission processes in emerging metal hexachloride scintillators $\text{Cs}_2\text{HfCl}_6$ and $\text{Cs}_2\text{ZrCl}_6$

V. Mykhaylyk,<sup>a</sup> S. S. Nagorny,<sup>b,c</sup> V. V. Nahorna,<sup>b,d</sup> P. Wang,<sup>b,d</sup> M. D. Frogley,<sup>a</sup> L. Swiderski,<sup>e</sup> V. Kolomiets<sup>f</sup> and L. Vasylychko<sup>g</sup>

Crystals of metal hexachlorides  $\text{Cs}_2\text{MCl}_6$  ( $M = \text{Hf}$  or  $\text{Zr}$ ) have recently emerged as promising materials for scintillation applications due to their excellent energy resolution. In this work, we investigated the crystal structure and scintillation properties of  $\text{Cs}_2\text{HfCl}_6$  and  $\text{Cs}_2\text{ZrCl}_6$  crystals in the broad temperature range from 9 to 300 K. X-ray diffraction data confirmed the same cubic structure (space group  $Fm\bar{3}m$ ) for  $\text{Cs}_2\text{HfCl}_6$  and  $\text{Cs}_2\text{ZrCl}_6$  over the entire examined temperature range. The room temperature scintillation light yield of  $\text{Cs}_2\text{HfCl}_6$  excited with a  $^{137}\text{Cs}$   $\gamma$ -source is measured to be 24 800 photons per MeV, while  $\text{Cs}_2\text{ZrCl}_6$  exhibits 33 900 photons per MeV resulting in energy resolutions of 5.3% and 4.5%, respectively. The alpha-to-beta ratio determined at room temperature for 5.5 MeV  $\alpha$ -particles from an  $^{241}\text{Am}$  source is equal to 0.39 for  $\text{Cs}_2\text{HfCl}_6$  and 0.35 for  $\text{Cs}_2\text{ZrCl}_6$ . The measurements of scintillation decay curves revealed complex kinetics due to delayed recombination processes. A tangible enhancement of the scintillation yield with heating is observed in the 125–150 K range. This effect is a manifestation of negative thermal quenching explained by thermal activation of trapped carriers. A model of the emission centre is proposed that consistently explains the observed changes of emission intensity with temperature in the crystals under study.

Received 23rd January 2022,  
Accepted 22nd March 2022DOI: [10.1039/d2dt00223j](https://doi.org/10.1039/d2dt00223j)[rsc.li/dalton](http://rsc.li/dalton)

## 1. Introduction

The scintillation method of detecting ionizing radiation and particles is broadly used in scientific research, nuclear security and medical diagnostics. The key component of any scintillation detector is the scintillating compound, whose properties often determine the performances of the detection technique. New scintillation materials with improved performance characteristics (such as a high light yield and superior energy resolution) are always sought after and, hence, their development is a vibrant area of scientific research. The materials that belong to the halide family remain the focus of attention and over the last decade many complex halide compounds with promising

characteristics have been discovered (see *e.g.* ref. 1 and reference therein). However, only a few materials showed potential for further development and commercialisation due to several reasons, *i.e.* difficulties in synthesis, hygroscopicity, poor consistency of performance and high production cost. It remains a challenge to find materials where these issues can be either avoided or alleviated.

Self-activated metal hexachloride scintillators<sup>2,3</sup> with a general formula  $\text{Cs}_2\text{MCl}_6$  ( $M = \text{Hf}$  or  $\text{Zr}$ ), are receiving a great deal of attention. The crystals have a simple structure and exhibit low hygroscopicity – two important properties that compare favourably with other halide scintillators. The first study of  $\text{Cs}_2\text{HfCl}_6$  carried out by Burger *et al.*<sup>2</sup> quoted an impressive light yield of 54 000 photons per MeV and 3.3% (FWHM) energy resolution for 662 keV  $\gamma$ -rays of  $^{137}\text{Cs}$ . The measurements of light yield with energy also revealed that this material has much better non-proportionality of scintillation response in comparison with other halide scintillators. Another important feature of  $\text{Cs}_2\text{MCl}_6$  scintillators is a low intrinsic radioactivity<sup>4</sup> making these compounds highly desirable for the experimental search of rare nuclear processes occurring in Hf and Zr.<sup>5</sup>

These findings triggered a significant interest in the scientific community and prompted research activity to improve the

<sup>a</sup>Diamond Light Source, Harwell Campus, Didcot, OX11 0DE, UK.E-mail: [vitaliy.mykhaylyk@diamond.ac.uk](mailto:vitaliy.mykhaylyk@diamond.ac.uk)<sup>b</sup>Arthur B. McDonald Canadian Astroparticle Physics Research Institute, Queen's University Kingston, ON, K7L 3N6, Canada<sup>c</sup>Departments of Physics, Engineering Physics and Astronomy, Queen's University Kingston, ON, K7L 3N6, Canada<sup>d</sup>Chemistry Department, Queen's University Kingston, ON, K7L 3N6, Canada<sup>e</sup>National Centre for Nuclear Research, Soltana 7, 05-400 Otwock, Poland<sup>f</sup>Physics Department I. Franko National University of Lviv, 50 Dragomanova Str., 79005 Lviv, Ukraine<sup>g</sup>Lviv Polytechnic National University, 12 Bandera Str., Lviv 79013, Ukraine

scintillation characteristics of  $\text{Cs}_2\text{MCl}_6$  crystals.<sup>6–8</sup> These efforts have been accompanied by extensive theoretical and experimental investigations of the scintillation mechanism which is attributed to the emission of self-trapped excitons (STE).<sup>9–12</sup> In these studies a special attention was paid to the effect of impurities and defects,<sup>13–17</sup> as well as cation and anion substitution<sup>7,18–21</sup> on the scintillation properties. Such a holistic approach enabled targeted optimisation of the manufacturing process that led to the production of large, high-quality scintillation crystals with the enhanced performance characteristics.<sup>22,23</sup>

Despite a significant number of recent studies on scintillation and luminescence properties of  $\text{Cs}_2\text{MCl}_6$ , the information on some physical characteristics of the crystals is incomplete and fragmented. To begin with, there is a lack of accurate crystallographic information for these compounds. The data on the crystal structure of  $\text{Cs}_2\text{HfCl}_6$  and  $\text{Cs}_2\text{ZrCl}_6$  published more than 40 years ago<sup>24,25</sup> reveal discrepancies of lattice parameters that hinder the identification of structures. Furthermore, no investigations on temperature changes of the crystal lattice have been published so far. This knowledge is essential to achieve a comprehensive insight into physical properties of the solids and especially for interpretation of their temperature dependence. Lastly, the scintillation properties of  $\text{Cs}_2\text{ZrCl}_6$  have not been studied to the same extent as these of  $\text{Cs}_2\text{HfCl}_6$ . Lack of such information motivated us to carry out systematic investigations of the crystal structure and scintillation properties of  $\text{Cs}_2\text{HfCl}_6$  and  $\text{Cs}_2\text{ZrCl}_6$  crystals in a broad temperature range from 9 to 300 K.

## 2. Materials and methods

### 2.1. Preparation of starting materials

Anhydrous  $\text{CsCl}$  (99.9%),  $\text{HfCl}_4$  (98%) and  $\text{ZrCl}_4$  (99.9%) powders were used as starting materials. Due to low initial purity of the  $\text{HfCl}_4$  and  $\text{ZrCl}_4$  powders they were subjected to a two-stage sublimation process prior to the synthesis. At the first stage, 50 g of raw  $\text{HfCl}_4$  or  $\text{ZrCl}_4$  powder was loaded into a quartz ampoules and sealed under vacuum. Then the sealed tube was placed into a horizontal furnace for sublimation at 400 °C for  $\text{HfCl}_4$  and 380 °C for  $\text{ZrCl}_4$ . After this stage, the yellow-white  $\text{HfCl}_4$  or  $\text{ZrCl}_4$  powders were separated from impurities of dark grey colour. At the second stage of purification, both  $\text{HfCl}_4$  and  $\text{ZrCl}_4$  powders were reloaded into new quartz ampoules and were then subjected to sublimation at a temperature of 300 °C. The final yields of the two stage purifications were 89% (44.3 g) and 90% (45 g) for  $\text{HfCl}_4$  and  $\text{ZrCl}_4$ , respectively.

As-received  $\text{CsCl}$  grains and purified  $\text{HfCl}_4$  or  $\text{ZrCl}_4$  powders were mixed in a stoichiometric ratio, thoroughly ground using a mortar and pestle, and then loaded into a tapered quartz ampoule with an inner diameter of 22 mm. Then mixture was dried by heating at 120 °C for 1 hour under vacuum. This was followed by the reduction stage at 300 °C for 1 hour under the

flow of hydrogen. The reduced materials were then sealed in the tapered quartz ampoule under a vacuum of  $5 \times 10^{-4}$  mbar.

### 2.2. Crystal production

$\text{Cs}_2\text{HfCl}_6$  and  $\text{Cs}_2\text{ZrCl}_6$  single crystals were grown by the vertical Bridgman technique. Sealed ampoules with prepared reagents were placed in a furnace and gradually heated to 850 °C. The ampoules were maintained at 850 °C for at least 20 hours prior to the crystal growth to form the  $\text{Cs}_2\text{HfCl}_6$  or  $\text{Cs}_2\text{ZrCl}_6$  stoichiometric compounds and to ensure melt homogeneity. Then, the first crystal growth was performed at a pulling rate of 2.7 mm per hour with a temperature gradient of 24 °C  $\text{cm}^{-1}$  at the solid–liquid interface in the case of  $\text{Cs}_2\text{HfCl}_6$ . In the case of  $\text{Cs}_2\text{ZrCl}_6$  the pulling rate was 1.5 mm per hour with the temperature gradient of 28 °C  $\text{cm}^{-1}$ . The obtained boules after this first fast growth were processed to remove all visual impurities or inclusions along with the first-to-freeze sections. The selected crystal pieces were loaded into a new quartz ampoule for the second growth. The second slow crystal growth was performed with pulling rate of 0.7 mm per hour with temperature gradient 42 °C  $\text{cm}^{-1}$  for the  $\text{Cs}_2\text{HfCl}_6$  compound, and at the pulling rate of 0.5 mm per hour with temperature gradient 25 °C  $\text{cm}^{-1}$  for  $\text{Cs}_2\text{ZrCl}_6$  crystal, correspondingly.

$\text{Cs}_2\text{HfCl}_6$  and  $\text{Cs}_2\text{ZrCl}_6$  crystals of 21 mm diameter and around 60 mm length were obtained (see Fig. 1). The crystal samples with dimensions 7 × 7 × 2 mm for the measurements of optical properties were cut from the tip of the boules by diamond wire saw, and then polished with 1200 grit sandpaper and mineral oil as a lubricant.

### 2.3. X-ray diffraction studies

The powder samples for X-ray diffraction studies were prepared by grinding the pieces of the crystals in an agate mortar. The sample was then mounted on an Oxford Cryosystems Phenix cold stage allowing measurements at 12–300 K under vacuum. The measurements were performed in a Rigaku SmartLab diffractometer with 9 kW rotating Cu-anode. The data were collected in angular range 10–90° with step 0.01° using a HyPix 3000 2D semiconductor detector. The structural parameters of the crystals were derived from full profile Rietveld refinement of the experimental XRD data using the WinCSD software package.<sup>26</sup> Unit cell dimensions, positional and displacement parameters of atoms were refined together with profile parameters, the texture coefficient in the [111] axis and corrections for absorption and instrumental sample shift.

### 2.4. Measurements of scintillation properties

For the measurement of pulse height spectra, polished cylindrical crystals of  $\text{Cs}_2\text{HfCl}_6$  and  $\text{Cs}_2\text{ZrCl}_6$  with dimensions 20 mm diameter × 12 mm were wrapped in Teflon tape and attached to the window of the photomultiplier tube (R6231-100 PMT, Hamamatsu Photonic, Japan) using an optical grease. The anode signal was sent to a Canberra 2005 preamplifier and then to an Ortec 672 shaping amplifier. The pulse height spectra were collected with 10 μs shaping time, uni-



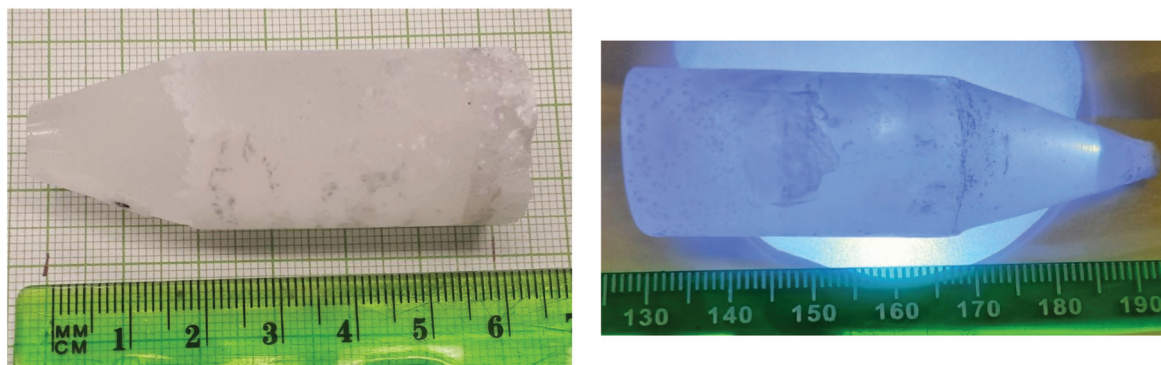


Fig. 1 Left panel:  $\text{Cs}_2\text{HfCl}_6$  single crystal (daylight illumination). Right panel:  $\text{Cs}_2\text{ZrCl}_6$  single crystalline boule (illumination by UV lamp). Both crystals have diameter 21 mm and 60 mm in length, with mass of about 60 g each.

polar output. The light yield is obtained by comparing the peak position of the photopeak with that of the single-electron spectrum. The spectra were acquired using a  $^{137}\text{Cs}$  source emitting 662 keV  $\gamma$ -rays. An additional  $^{241}\text{Am}$  source emitting 5.5 MeV  $\alpha$ -particles was used for measurements of alpha-to-beta ratio.

To study scintillation properties with temperature,  $7 \times 7 \times 2$  mm polished samples of the crystals were placed in a helium cryostat and excited by 5.5 MeV  $\alpha$ -particles from an  $^{241}\text{Am}$  source. The scintillation pulses were detected by a multi-alkali photomultiplier tube (PMT) model 9124A (Electron Tube Enterprises, UK). A fast ADC with 10 ns sampling interval was used to digitize the signal from the PMT. This allows resolving individual photons and recording single photon signals. To capture the slow decay component that makes a tangible contribution to the scintillation pulse at low temperature, the signal was recorded over 700  $\mu\text{s}$ . The set of recorded scintillation events (*ca.* 2000) was then analysed off-line. The customised analysis software calculates two histograms: pulse height distribution and distribution of photon arrival times. The first is the measure of a scintillation light yield while the second represents a scintillation decay curve.<sup>27</sup> The measurements were carried out while cooling the crystal to avoid contribution from thermally released charge carriers to the scintillation event observed during heating.

## 3. Results and discussion

### 3.1 Crystal structure characterisation with temperature

Fig. 2 shows XRD patterns of the samples measured *in situ* in the temperature range 12–300 K. Analysis of the XRD data revealed that, in addition to the main  $\text{Cs}_2\text{HfCl}_6$  and  $\text{Cs}_2\text{ZrCl}_6$  phases, both measured samples contain the admixture phase of CsCl. The appearance of this phase in  $\text{Cs}_2\text{HfCl}_6$  has previously been explained by incomplete reaction between starting materials due to the high vapor pressure of  $\text{HfCl}_4$ .<sup>20</sup>

Inspection of the XRD patterns for the  $\text{Cs}_2\text{HfCl}_6$  sample reveals the abnormal relative intensity of several Bragg's maxima, especially pronounced for the [111] direction, indicat-

ing strong preferred particle orientations (texture) in the analyzed powder sample. This effect is often observed for powder samples prepared by grinding a bulk single crystal. A similar, though less pronounced, texture effect was also observed in the  $\text{Cs}_2\text{ZrCl}_6$  sample.

Cooling the samples down to 12 K does not affect the crystal structure and phase composition of the materials. Besides the gradual shift of the Bragg's peak positions due to the lattice contraction, no other visible changes like a reflection splitting and/or appearance of additional peaks were observed in the XRD patterns of  $\text{Cs}_2\text{HfCl}_6$  and  $\text{Cs}_2\text{ZrCl}_6$  collected at different temperatures (Fig. 2).

Structural parameters of the  $\text{Cs}_2\text{HfCl}_6$  and  $\text{Cs}_2\text{ZrCl}_6$  phases at different temperatures were derived from the corresponding experimental XRD data by a full profile Rietveld refinement. In this procedure, the lattice parameters, atom coordinates and displacement parameters  $B_{\text{iso}}$  in the main  $\text{Cs}_2\text{HfCl}_6$  and  $\text{Cs}_2\text{ZrCl}_6$  structures (space group  $Fm\bar{3}m$ ) were refined together with the profile parameters, the texture coefficient for [111] axis and corrections for absorption and the instrumental sample shift. For the minor CsCl phase only lattice parameters were refined. As a starting model for the Rietveld refinement we adopted the atomic positions of the  $\text{Cs}_2\text{HfCl}_6$  structure from ref. 24. The refinement procedure led to a good fit between experimental and calculated profiles in all cases. Examples of the Rietveld refinement for  $\text{Cs}_2\text{HfCl}_6$  and  $\text{Cs}_2\text{ZrCl}_6$  structures at the selected temperatures are shown in Fig. 3. Obtained structural parameters for  $\text{Cs}_2\text{HfCl}_6$  and  $\text{Cs}_2\text{ZrCl}_6$  at 300 and 12 K are summarized in Tables 1 and 2.

The crystal structure of  $\text{Cs}_2\text{MCl}_6$  ( $M = \text{Hf}, \text{Zr}$ ) can be viewed as a variant of the ideal perovskite with the nominal composition  $\text{ABX}_3$ , where half of the B sites are vacant and the  $\text{BX}_6$ -octahedra are isolated from one another. Caesium atoms are coordinated by twelve Cl atoms and fill the voids between the  $\text{MCl}_6$  octahedra<sup>28</sup> as shown in Fig. 4. These features of the crystal structure recently inspired the dedicated term – vacancy-ordered double perovskites.<sup>29</sup>

Room temperature lattice parameters of  $\text{Cs}_2\text{HfCl}_6$  and  $\text{Cs}_2\text{ZrCl}_6$  obtained in this work are in good agreement with the



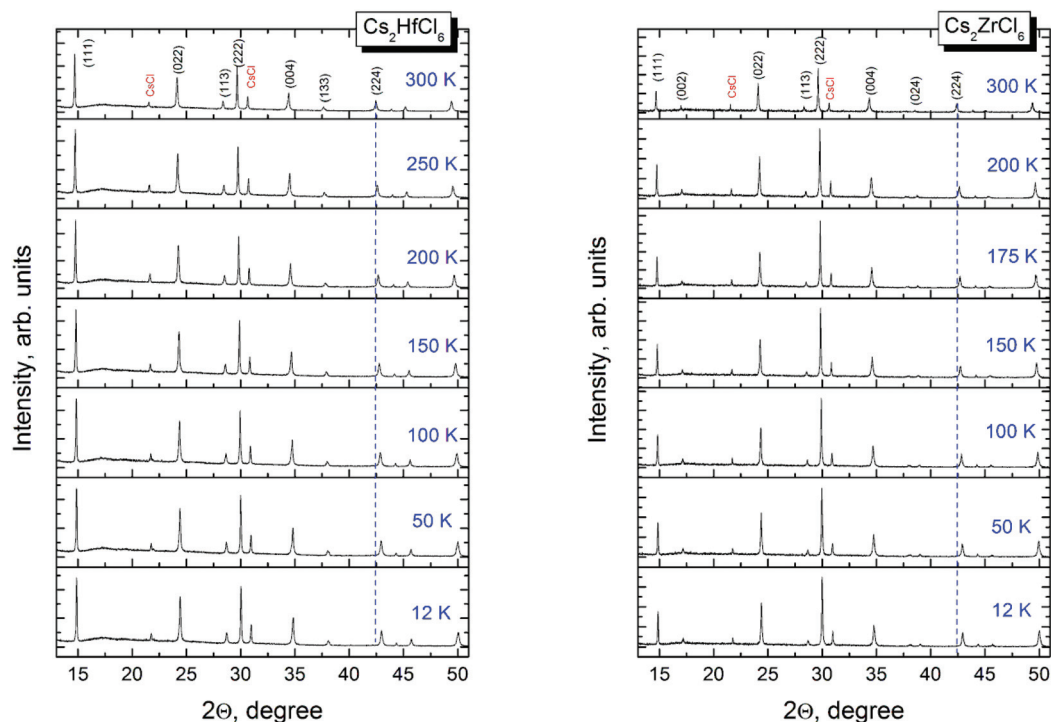


Fig. 2 Evolution of XRD patterns of  $\text{Cs}_2\text{HfCl}_6$  and  $\text{Cs}_2\text{ZrCl}_6$  on cooling from 300 K to 12 K. Miller's indices for the corresponding  $Fm\bar{3}m$  cubic structures and peaks from the CsCl parasitic phase are labelled in the top panels. Vertical dashed lines serve as guide for tracking the shift of Bragg's maxima.

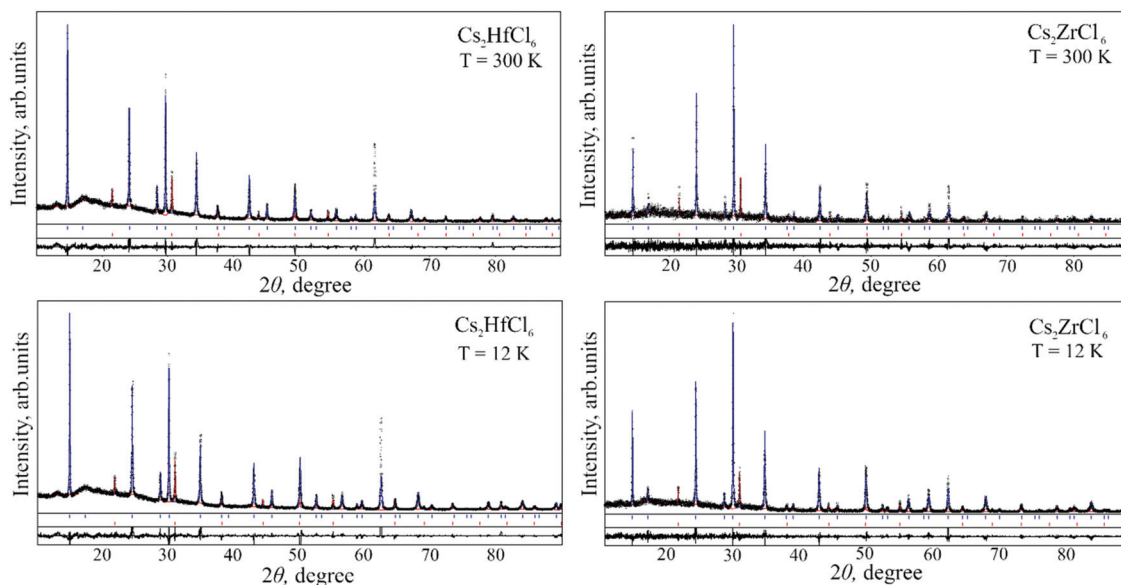


Fig. 3 Graphical results of the Rietveld refinement of  $\text{Cs}_2\text{HfCl}_6$  and  $\text{Cs}_2\text{ZrCl}_6$  samples at 300 K and 12 K. Experimental XRD patterns (black dots) are shown in comparison with calculated patterns for the main  $\text{Cs}_2\text{MCl}_6$  (blue) and admixture CsCl (red) phases. Short vertical bars below the diagrams indicate the positions of Bragg's maxima in corresponding structures.

structural data for these compounds published in ref. 24 and 30, respectively (see Fig. 5). In contrast, the unit cell dimensions of these compounds reported in ref. 25 look rather underestimated. In ref. 31 the lattice parameter of

$\text{Cs}_2\text{ZrCl}_6$  was predicted based on an empirical model describing the unit cell dimension of cubic  $\text{A}_2\text{MX}_6$  crystals as a linear function of the ionic radii and electronegativity of the constituting ions.

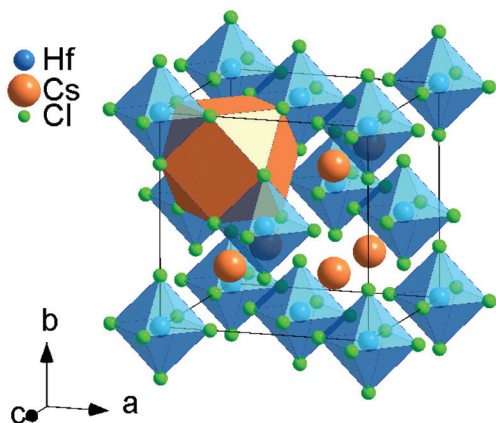


**Table 1** Structural parameters of Cs<sub>2</sub>HfCl<sub>6</sub> at 12 K and 300 K (space group *Fm3m*)

Lattice parameter, Å	Atoms, sites	<i>x</i>	<i>y</i>	<i>z</i>	<i>B</i> <sub>iso</sub> , Å <sup>2</sup>
<i>T</i> = 12 K ( <i>R</i> <sub>1</sub> = 0.152, <i>R</i> <sub>p</sub> = 0.254)					
10.2990(3)	Hf, 4 <i>a</i>	0	0	0	0.29(8)
	Cs, 8 <i>c</i>	1/4	1/4	1/4	0.93(8)
	Cl, 24 <i>e</i>	0.2502(7)	0	0	1.63(15)
Texture axis and parameter: [111] 0.055(1)					
<i>T</i> = 300 K ( <i>R</i> <sub>1</sub> = 0.103, <i>R</i> <sub>p</sub> = 0.266)					
10.4208(3)	Hf, 4 <i>a</i>	0	0	0	0.51(9)
	Cs, 8 <i>c</i>	1/4	1/4	1/4	2.18(11)
	Cl, 24 <i>e</i>	0.2499(6)	0	0	1.63(15)
Texture axis and parameter: [111] 0.060(1)					

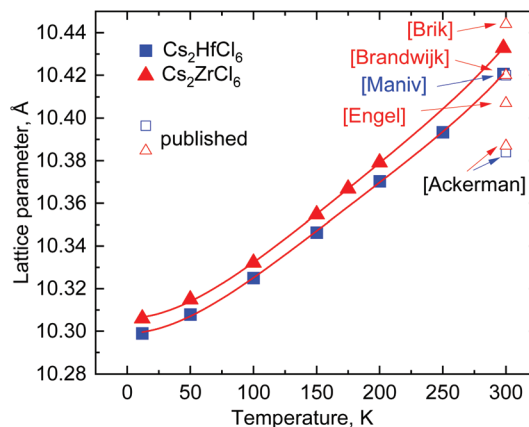
**Table 2** Structural parameters of Cs<sub>2</sub>ZrCl<sub>6</sub> at 12 K and 300 K (space group *Fm3m*)

Lattice parameter, Å	Atoms, sites	<i>x</i>	<i>y</i>	<i>z</i>	<i>B</i> <sub>iso</sub> , Å <sup>2</sup>
<i>T</i> = 12 K ( <i>R</i> <sub>1</sub> = 0.066, <i>R</i> <sub>p</sub> = 0.248)					
10.3060(3)	Zr, 4 <i>a</i>	0	0	0	0.31(8)
	Cs, 8 <i>c</i>	1/4	1/4	1/4	0.46(4)
	Cl, 24 <i>e</i>	0.2321(4)	0	0	0.49(8)
Texture axis and parameter: [111] 0.132(3)					
<i>T</i> = 300 K ( <i>R</i> <sub>1</sub> = 0.134, <i>R</i> <sub>p</sub> = 0.461)					
10.4331(6)	Zr, 4 <i>a</i>	0	0	0	1.4(2)
	Cs, 8 <i>c</i>	1/4	1/4	1/4	0.79(8)
	Cl, 24 <i>e</i>	0.2248(8)	0	0	0.5(2)
Texture axis and parameter: [111] 0.134(6)					

**Fig. 4** Polyhedral view of the Cs<sub>2</sub>HfCl<sub>6</sub> structure showing isolated [HfCl<sub>6</sub>] octahedra and [CsCl<sub>12</sub>] cubooctahedron.

Taking into account that members of this family may exhibit structural instability,<sup>32</sup> it was important to check for a possible phase transition at low temperatures. Our structural studies confirmed the same cubic structure (space group *Fm3m*) for Cs<sub>2</sub>HfCl<sub>6</sub> and Cs<sub>2</sub>ZrCl<sub>6</sub> over the whole examined temperature range.

Fig. 5 shows that cooling the samples causes only gradual decrease of the lattice constant due to thermal contraction of the crystals. No anomalies pointing to possible changes of the

**Fig. 5** The temperature dependence of the lattice parameters of Cs<sub>2</sub>HfCl<sub>6</sub> and Cs<sub>2</sub>ZrCl<sub>6</sub>. For comparison the published values of the lattice parameters are shown as open blue squares (Cs<sub>2</sub>HfCl<sub>6</sub>) and open red triangles (Cs<sub>2</sub>ZrCl<sub>6</sub>). The red lines display fitting of the experimental data to the eqn (1).

crystal structure of these materials are observed in the low temperature range. The measured temperature dependencies of the lattice parameters are fitted using a nonlinear function:<sup>33</sup>

$$a(T) = a_0(1 + a_1T^2 + a_2T^3 + a_3T^4) \quad (1)$$

where *a*<sub>0</sub> is lattice size at *T* = 0 K, *a*<sub>1</sub>...*a*<sub>3</sub> are fitting constants. The parameters of the fitting are given in Table 3.

### 3.2. Scintillation response at room temperature

To attest the scintillation performance of Cs<sub>2</sub>HfCl<sub>6</sub> and Cs<sub>2</sub>ZrCl<sub>6</sub> crystals we first measured their scintillation response at room temperature using a  $\gamma$ -ray source. The energy resolution (FWHM) and relative light yield were derived from the pulse height spectra of the crystals obtained at 662 keV  $\gamma$ -rays excitation from a <sup>137</sup>Cs source (Fig. 6). In addition to the well resolved 662 keV photopeak the spectra show the Compton continuum, a backscatter peak and a peak at 32 keV corresponding to X-rays from barium emitted during decay of <sup>137</sup>Cs. The obtained values of relative light yield and the energy resolution of the crystals are summarised in the Table 4. These results show that the relative light yield and energy resolution of Cs<sub>2</sub>HfCl<sub>6</sub> crystal measured in this work is inferior in comparison with the published results. In contrast, Cs<sub>2</sub>ZrCl<sub>6</sub> exhibits much higher light yield 33 900 ± 1700 ph per MeV than previously reported (25 100 ± 1200 ph per MeV (ref. 3)) and very encouraging energy resolution 4.5%. This finding demonstrates that Cs<sub>2</sub>ZrCl<sub>6</sub> scintillator is well suited for

**Table 3** Parameters of the fit for temperature dependence of lattice constants of Cs<sub>2</sub>HfCl<sub>6</sub> and Cs<sub>2</sub>ZrCl<sub>6</sub> crystals obtained using eqn (1)

Crystal	<i>a</i> <sub>0</sub> , Å	<i>a</i> <sub>1</sub> × 10 <sup>-7</sup>	<i>a</i> <sub>2</sub> × 10 <sup>-9</sup>	<i>a</i> <sub>3</sub> × 10 <sup>-12</sup>
Cs <sub>2</sub> HfCl <sub>6</sub>	10.2991(7)	3.76(21)	-1.44(16)	2.10(33)
Cs <sub>2</sub> ZrCl <sub>6</sub>	10.3061(5)	3.71(21)	-1.36(18)	1.95(37)



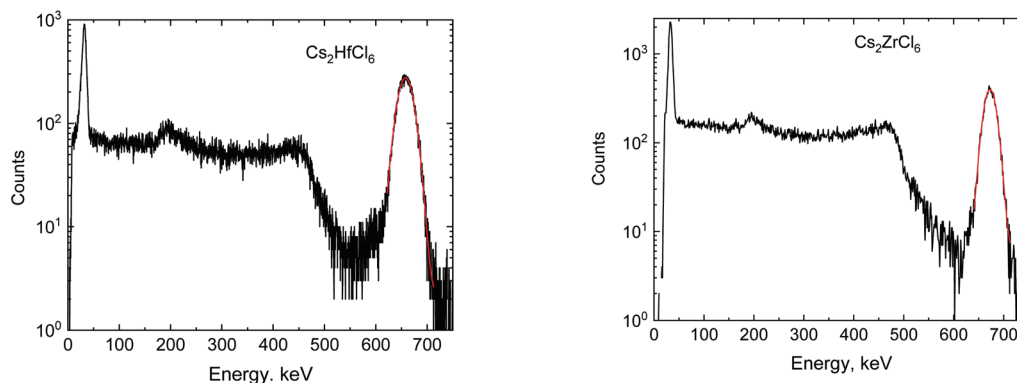


Fig. 6 Pulse height spectra of  $\text{Cs}_2\text{HfCl}_6$  and  $\text{Cs}_2\text{ZrCl}_6$  scintillators measured during excitation by 662 keV  $\gamma$ -rays of  $^{137}\text{Cs}$  source (shaping time is equal to 10  $\mu\text{s}$ ). The red line shows the Gaussian fit of the photopeak.

Table 4 Scintillation characteristics of  $\text{Cs}_2\text{HfCl}_6$  and  $\text{Cs}_2\text{ZrCl}_6$  crystals at 9 and 295 K

Crystal	Light yield <sup>a</sup> , ph per MeV		Light yield, ph per MeV	Energy resolution, %	Alpha-to-beta ratio	Scintillation pulse decay constants <sup>b</sup> , $\mu\text{s}$						Ref.		
	295 K	9 K				295 K			9 K					
			$\tau_1$	$\tau_2$	$\tau_3$	$\tau_1$	$\tau_2$	$\tau_3$						
$\text{Cs}_2\text{HfCl}_6$	19 600	25 700	24 800	5.3	0.39	0.4	5.1	15.2	0.6	12.0	76.0	This work		
			54 000	3.3		0.3	4.4	n.d.					2	
			30 000	3.3		0.4	3.9	n.d.						20
			36 400	4.1		0.9	4.4	n.d.						
			26 800	4.3		1.0	5.0	12.0						16
$\text{Cs}_2\text{ZrCl}_6$	31 150	35 800	33 900	4.5	0.35	0.4	2.7	12.5	1.1	18.7	95.0	This work		
			25 100	n.d.		1.5	7.5	n.d.					3	

n.d. – not detected. <sup>a</sup>The relative light yield determined during excitation by 5.5 MeV alpha particles of  $^{241}\text{Am}$  is converted to the light yield corresponding to gamma quanta based on alpha-to-beta ratios of the crystals. <sup>b</sup>Scintillation decay constants measured under irradiation by 5.5 MeV alpha particles of  $^{241}\text{Am}$ .

$\gamma$ -spectroscopy. The obtained alpha-to-beta ratio (or quenching factor) is similar for both crystals and close to that reported in the literature.<sup>34</sup>

It should be noted that the values presented in Table 4 were obtained with the shaping time equal to 10  $\mu\text{s}$ . Increasing the shaping time from 0.5 to 10  $\mu\text{s}$  results in a significant augmentation of the detected relative light yield: it quadrupled in  $\text{Cs}_2\text{HfCl}_6$  and increased by factor of 7 in  $\text{Cs}_2\text{ZrCl}_6$ . This is due to the strong contribution of the slow decay components to the scintillation pulses constituting *ca.* 50% of the total intensity (see also discussion in sec. 3.3). The obtained results also evidence that the fractional contribution of this slow component is much stronger in  $\text{Cs}_2\text{ZrCl}_6$ .

### 3.3. Scintillation light output and decay time with temperature

To examine the behaviour of  $\text{Cs}_2\text{MCl}_6$  crystal scintillators over a wide temperature range we measured the temperature dependence of the light output under  $\alpha$ -particle excitation over 9–295 K. The crystals exhibit a very strong scintillation response manifested as clearly resolved peaks from  $\alpha$ -particles

of  $^{241}\text{Am}$ . The pulse height spectra of the crystals at different temperatures are shown in Fig. 7.

The scintillation response of a reference material,  $\text{CaWO}_4$  (provided by Institute of Single Crystals SRC “Carat” Lviv, Ukraine), and the measured values of alpha-to-beta ratio at room temperatures were used to derive the light yield of the crystals under study, in the same way as described in ref. 12. The scintillation light yields obtained for  $\text{Cs}_2\text{HfCl}_6$  and  $\text{Cs}_2\text{ZrCl}_6$  crystals under  $\alpha$ -particle excitation are  $19\,600 \pm 2900$  photons per MeV and  $31\,150 \pm 3700$  photons per MeV, respectively (see Table 4). Both values are slightly less than that measured with the  $\gamma$ -source. This discrepancy could be due to the applied conversion procedure that assumes identical light collection from the reference and test crystals.<sup>12</sup> This assumption does not account for the difference in optical properties of materials (refraction, absorption, and scattering) affecting the light collection and leads to underestimation of the scintillation light yield.<sup>35</sup>

The measurements with varying temperature revealed unusual dependencies of scintillation light output in both crystals (Fig. 8). They are distinctly different to the gradual



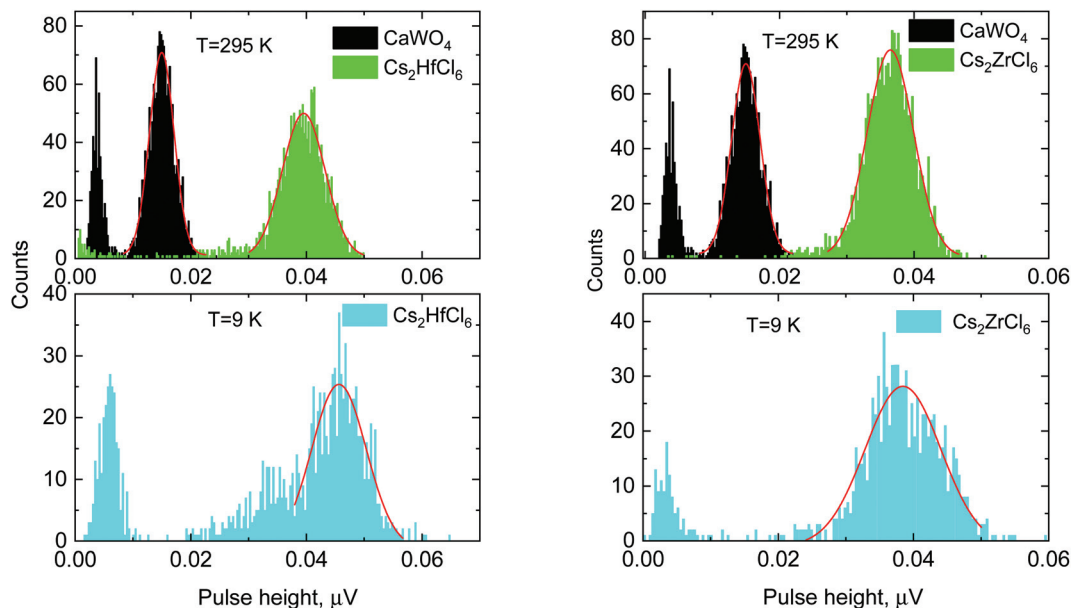


Fig. 7 Pulse height spectra of  $\text{Cs}_2\text{HfCl}_6$  and  $\text{Cs}_2\text{ZrCl}_6$  scintillators measured at 295 and 9 K during excitation by 5.5 MeV alpha particles of  $^{241}\text{Am}$ . The red lines show the Gaussian peak fits.

decrease of scintillation light yield observed with increasing temperature in the majority of undoped scintillators.<sup>36</sup> The light output of  $\text{Cs}_2\text{MCl}_6$  initially decreases with heating, but after reaching a minimum at *ca.* 100 K it increases. The trend changes again around 130 K after which the light output shows gradual decrease with temperature.

This feature is particularly evident in  $\text{Cs}_2\text{ZrCl}_6$  crystals which exhibits *ca.* 50% increase of the light yield at  $T = 125$  K in comparison with that at room temperature. It should be noted that this behavior of the emission intensity with temperature is very similar to that reported recently in ref. 10 and 12 where the decrease of the light yield observed below 100 K was attributed to the freeze-out of  $V_{\text{K}}$ -centers involved in the emission of self-trapped excitons (STE) in the crystals.

This type of temperature dependence termed as a “negative thermal quenching” has been observed before in some materials<sup>37</sup> including scintillators.<sup>38,39</sup> Assuming thermally acti-

vated crossover as the main mechanism that controls the population of involved states, this behavior can be explained by the thermal activation of intermediate trap states that leads to the enhancement of the emission intensity with increasing temperature. This can occur before the onset of non-radiative thermal quenching that causes a gradual decrease of emission intensity or during such quenching. In the presence of such processes, the model developed in ref. 37 gives the following expression for the temperature dependence of the emission intensity:

$$I(T) = I_0 \frac{1 + D_1 \exp\left(-\frac{E'_1}{kT}\right)}{1 + C_1 \exp\left(-\frac{E_1}{kT}\right) + C_2 \exp\left(-\frac{E_2}{kT}\right)}. \quad (2)$$

In eqn (2),  $I_0$  is the total emission intensity at zero temperature,  $D_1$ ,  $C_1$  and  $C_2$  are the transition rate constants,  $E'_1$  is the

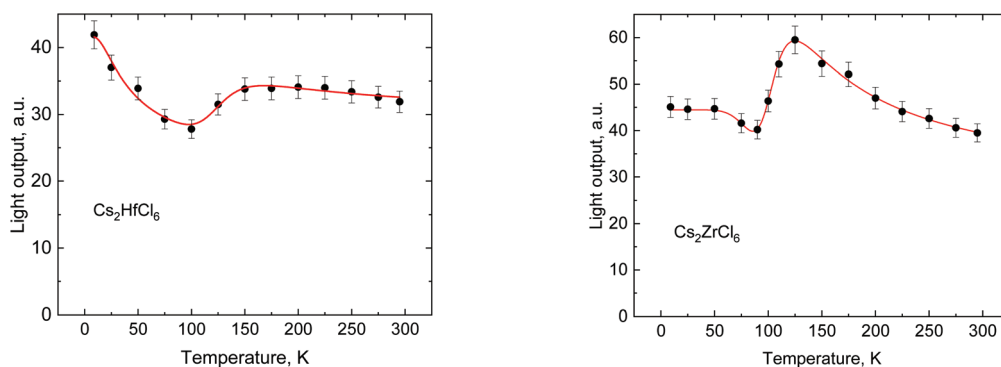


Fig. 8 Temperature dependence of the scintillation light output of  $\text{Cs}_2\text{HfCl}_6$  and  $\text{Cs}_2\text{ZrCl}_6$  measured under excitation by 5.5 MeV alpha particles from an  $^{241}\text{Am}$  source. The red lines show fits of eqn (2) to the experimental results using parameters from Table 5.



activation energy necessary to promote the trapped particles to the emission state,  $E_1$  and  $E_2$  are the activation energies for the non-radiative quenching and  $k$  is the Boltzmann constant. Thus, the numerator is responsible for the emission enhancement due to the thermal release of particles from the intermediate traps to the emitting states. In turn, the denominator describes the processes of thermally activated non-radiative quenching of the emitting state.

Eqn (2) was used to fit the data in Fig. 8 demonstrating a good agreement between the experimental results and theoretical model. The parameters of the fit are summarised in Table 5. The attribution of intermediate levels to hole trapping centres has already been established in these materials.<sup>10,12,17</sup> The values of activation energy  $E'_1$  (0.11 and 0.12 eV in  $\text{Cs}_2\text{HfCl}_6$  and  $\text{Cs}_2\text{ZrCl}_6$ , respectively) correlate well with the activation energy of  $V_k$ -centres further supporting the earlier assumption that the carriers released in this process are the cause of increase of the light yield.

The parameters obtained from the analysis of temperature-dependent light yield reveal an interesting feature: in both crystals the energy required to promote the trapped particles to the emission state  $E'_1$  is significantly larger than the first activation energy of thermal quenching  $E_1$  while it is very close to the value of the second activation energy  $E_2$ . The observed features of temperature dependence of the light yield can be explained using the schematic configuration coordinate diagram in Fig. 9. In the proposed model, the non-radiative quenching due to crossover from the excited to the ground state that requires activation energy  $E_1$  starts at low temperature (process 1). As the temperature increases, the thermal energy of the system reaches value  $E'_1$  enabling promotion of the trapped particle to the emitting level (process 2) and enhancing the emission intensity. Further increase of temperature enables straight depletion of intermediate traps through the thermally activated two-step process – from traps to the excited state and then crossover to the ground state (process 3) – leading to the decrease of emission intensity. Fig. 9 also reveals that the energy  $E_2$  needed to activate trap depletion should be equal to the sum  $E'_1 + E_1$ . It is worth noting that the values of the activation energies derived from the fitting to the model fulfil this condition within the uncertainties.

Fig. 10 shows the scintillation decay curves of  $\text{Cs}_2\text{HfCl}_6$  and  $\text{Cs}_2\text{ZrCl}_6$  crystals measured at different temperatures. The

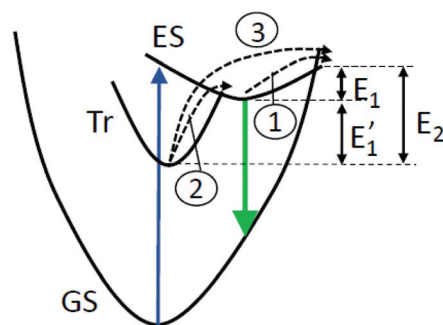


Fig. 9 Configuration coordinate diagram explaining the temperature dependence of luminescence in  $\text{Cs}_2\text{HfCl}_6$  and  $\text{Cs}_2\text{ZrCl}_6$ . The vertical blue and green lines show excitation and emission transitions between ground state (GS) and excited state (ES) of the emission centre. The dotted lines represent the thermally-activated processes: 1- crossover from the excited to the ground state, 2- activation of traps (Tr) and 3- non-radiative decay of the traps via two-step activation and crossover to the ground state.

measured decay curves display a complex non-single exponential shape that is a characteristic feature of decay kinetics due to a superposition of a few recombination processes. The decay curves were fitted using three exponential functions that ensure the best quality of the fit in the entire range of temperatures. It should be noted though, that in the case of complex decay, such fits are merely a way of quantifying the measured decay curves and the fit parameters are not directly related to the specific emission processes occurring in the material.

The numerical values derived from the fit are presented in Fig. 11 and 12. Comparison of the parameters reveals a pronounced change of decay rate with temperature in  $\text{Cs}_2\text{ZrCl}_6$ . In  $\text{Cs}_2\text{HfCl}_6$  only the slow decay time constant ( $\tau_3$ ) exhibits noticeable increase with cooling from room temperature to 200 K, while other decay time constants are mildly affected (see Fig. 11, left). The fractional content of amplitudes also changes insignificantly within *ca.*  $\pm 10\%$  with temperature (see Fig. 11, right). In contrast, for  $\text{Cs}_2\text{ZrCl}_6$  all decay time constants and amplitudes experience tangible changes with cooling from room temperature as is demonstrated in Fig. 12.

An interesting feature is observed in  $\text{Cs}_2\text{ZrCl}_6$  at 125 K. The decay time constants exhibit a prompt twofold rise followed by a quick drop. Since this feature correlates in temperature with the increase of the scintillation light output, we consider this observation as another manifestation of above-mentioned processes of the thermal activation of emission centers. Release of trapped charges at this temperature causes not only increase of the scintillation intensity but also slows down the emission. Once it is completed, the emission rate is accelerating again due to thermal quenching. This is accompanied by the changes in the fractional content of the fast and the slow decay components. Comprehensive modelling of intensity evolution with time and temperature in these materials is known to be a challenging task<sup>10,11</sup> that is beyond the scope of present study.

Table 5 Parameters of the fit obtained from the temperature dependence of the scintillation light output of  $\text{Cs}_2\text{HfCl}_6$  and  $\text{Cs}_2\text{ZrCl}_6$  crystals using eqn (2)

Parameter	$\text{Cs}_2\text{HfCl}_6$	$\text{Cs}_2\text{ZrCl}_6$
$I_0$	41.6(9)	44.4(6)
$D_1$	$2.1 \times 10^4$	$2.1 \times 10^6$
$E'_1$ , eV	0.11(5)	0.12(8)
$C_1$	0.84	105
$E_1$ , eV	0.005(1)	0.043(14)
$C_2$	$3.1 \times 10^4$	$3.3 \times 10^6$
$E_2$ , eV	0.11(5)	0.13(7)



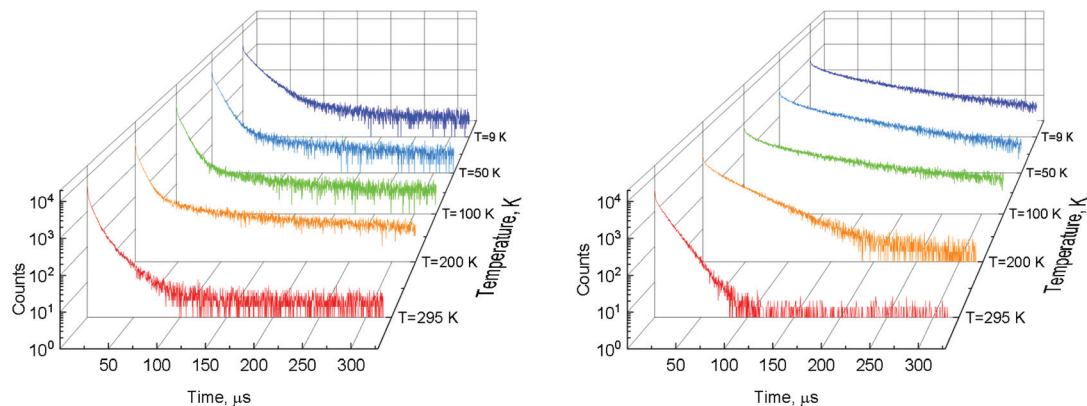


Fig. 10 Scintillation decay curves of  $\text{Cs}_2\text{HfCl}_6$  (left) and  $\text{Cs}_2\text{ZrCl}_6$  (right) crystals measured at different temperatures under excitation by 5.5 MeV alpha particles of an  $^{241}\text{Am}$  source.

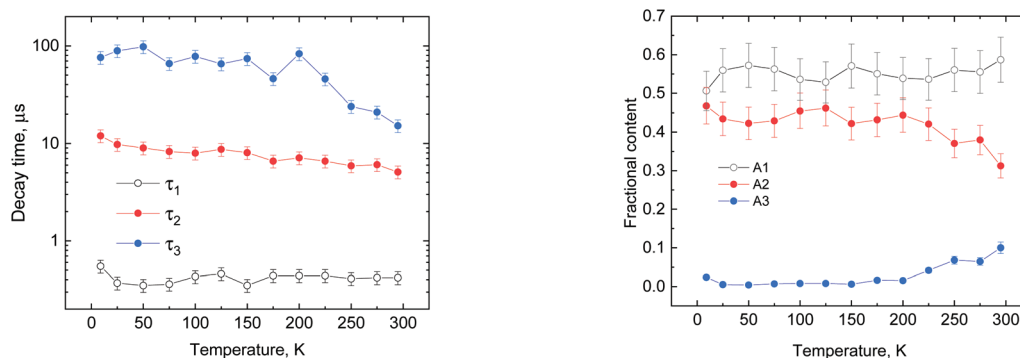


Fig. 11 Temperature dependence of decay time constants (left) and their amplitudes (right) obtained from the fitting of the decay curves of  $\text{Cs}_2\text{HfCl}_6$ , by a sum of three exponential functions.

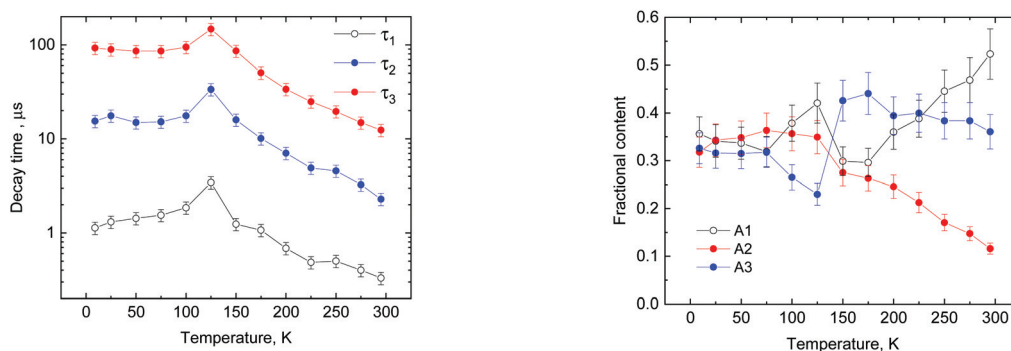


Fig. 12 Temperature dependence of decay time constants (left) and their amplitudes (right) obtained from the fitting of the decay curves of  $\text{Cs}_2\text{ZrCl}_6$  by a sum of three exponential functions.

## 4. Conclusions

Metal hexachloride crystals  $\text{Cs}_2\text{MCl}_6$  ( $\text{M} = \text{Hf}, \text{Zr}$ ) belong to a new class of materials with promising scintillation characteristics. For scintillation applications, it is important to understand and control the quality and emission properties of the crystals. In this work we investigated the crystal structure and

scintillation properties of  $\text{Cs}_2\text{HfCl}_6$  and  $\text{Cs}_2\text{ZrCl}_6$  over a wide (12–300 K) temperature range. XRD analysis revealed a gradual decrease of lattice parameters with cooling over this temperature range, ruling out the possibility of phase transition in the crystals. We measured the relative light yield, energy resolution and alpha-to-beta ratio of these scintillators at room temperature. The light yield of  $\text{Cs}_2\text{HfCl}_6$  under excitation with a  $^{137}\text{Cs}$   $\gamma$ -source



is found to be  $24\,800 \pm 1200$  photons per MeV along with 5.3% energy resolution.  $\text{Cs}_2\text{ZrCl}_6$  exhibits a higher light yield,  $33\,900 \pm 1700$  photons per MeV, resulting in an excellent energy resolution of 4.5%. The alpha-to-beta ratios determined with 5.5 MeV  $\alpha$ -particles of an  $^{241}\text{Am}$  source are equal to  $0.39 \pm 0.02$  and  $0.35 \pm 0.02$  for  $\text{Cs}_2\text{HfCl}_6$  and  $\text{Cs}_2\text{ZrCl}_6$  crystals, respectively.

The evolution of the scintillation light output and decay characteristics of the crystals with temperature was investigated under excitation with 5.5 MeV  $\alpha$ -particles of  $^{241}\text{Am}$ . We observed a significant enhancement of the light output in the 125–150 K temperature range that is attributed to a negative thermal quenching. The effect is explained as a thermal activation of the intermediate trap states that leads to the population of excited states. A consistent interpretation of the temperature changes in these crystals was achieved in a generalized phenomenological model. Using this model, we derived the numerical parameters that quantify the individual processes and constructed the energy scheme of the emission centre. The results of these studies provide better understanding of thermal changes in these crystalline materials. The results also motivate more in-depth study of the physical properties of these materials and underpin the strategy for development of scintillators with improved performance characteristics.

## Conflicts of interest

The authors declare no conflict of interest.

## Acknowledgements

L. V. acknowledges support of the National Research Foundation of Ukraine under grant no. 2020.02/0373 “Crystalline phosphors’ engineering for biomedical applications, energy saving lighting and contactless thermometry”. S. S. N., V. V. N. and P. W. are supported by the Arthur B. McDonald Canadian Astroparticle Physics Research Institute, with equipment funded by the Canada Foundation for Innovation and the Province of Ontario and housed at the Queen’s Centre for Advanced Computing. Research at the Perimeter Institute is supported by the Government of Canada through the Department of Innovation, Science, and Economic Development, and by the Province of Ontario. We would like to thank Dr G. Stenning for XRD measurements on the Rigaku SmartLab diffractometer in the Materials Characterisation Laboratory at the ISIS Neutron and Muon Source.

## References

- C. Dujardin, E. Auffray, E. Bourret-Courchesne, P. Dorenbos, P. Lecoq, M. Nikl, A. N. Vasil'ev, A. Yoshikawa and R. Y. Zhu, Needs, Trends, and Advances in Inorganic Scintillators, *IEEE Trans. Nucl. Sci.*, 2018, **65**, 1977–1997.
- A. Burger, E. Rowe, M. Groza, K. M. Figueroa, N. J. Cherepy, P. R. Beck, S. Hunter and S. A. Payne, Cesium hafnium chloride: A high light yield, non-hygroscopic cubic crystal scintillator for gamma spectroscopy, *Appl. Phys. Lett.*, 2015, **107**, 143505.
- K. Saeki, Y. Fujimoto, M. Koshimizu, T. Yanagida and K. Asai, Comparative study of scintillation properties of  $\text{Cs}_2\text{HfCl}_6$  and  $\text{Cs}_2\text{ZrCl}_6$ , *Appl. Phys. Express*, 2016, **9**, 042602.
- C. Cardenas, A. Burger, M. L. DiVacri, B. Goodwin, M. Groza, M. Laubenstein, S. Nagorny, S. Nisi and E. Rowe, Internal contamination of the  $\text{Cs}_2\text{HfCl}_6$  crystal scintillator, *Nucl. Instrum. Methods Phys. Res., Sect. A*, 2017, **872**, 23–27.
- V. Caracciolo, S. S. Nagorny, P. Belli, R. Bernabei, F. Cappella, R. Cerulli, A. Incicchitti, M. Laubenstein, V. Merlo, S. Nisi and P. Wang, Search for alpha decay of naturally occurring Hf-nuclides using a  $\text{Cs}_2\text{HfCl}_6$  scintillator, *Nucl. Phys. A*, 2020, **1002**, 121941.
- C. Delzer, M. Zhuravleva, L. Stand, C. Melcher, N. Cherepy, S. Payne, R. Sanner and J. P. Hayward, Observations regarding inclusions in the growth of  $\text{Cs}_2\text{HfCl}_6$  single crystal scintillators, *J. Cryst. Growth*, 2020, **531**, 125336.
- R. Hawrami, E. Ariesanti, V. Buliga, S. Motakef and A. Burger, Latest Progress on Advanced Bridgman Method-Grown  $\text{K}_2\text{PtCl}_6$  Cubic Structure Scintillator Crystals, *IEEE Trans. Nucl. Sci.*, 2020, **67**, 1020–1026.
- E. Ariesanti, R. Hawrami, A. Burger and S. Motakef, Improved growth and scintillation properties of intrinsic, non-hygroscopic scintillator  $\text{Cs}_2\text{HfCl}_6$ , *J. Lumin.*, 2020, **217**, 116784.
- B. Kang and K. Biswas, Carrier Self-trapping and Luminescence in Intrinsically Activated Scintillator: Cesium Hafnium Chloride ( $\text{Cs}_2\text{HfCl}_6$ ), *J. Phys. Chem. C*, 2016, **120**, 12187–12195.
- R. Kral, V. Babin, E. Mihokova, M. Buryi, V. V. Laguta, K. Nitsch and M. Nikl, Luminescence and Charge Trapping in  $\text{Cs}_2\text{HfCl}_6$  Single Crystals: Optical and Magnetic Resonance Spectroscopy Study, *J. Phys. Chem. C*, 2017, **121**, 12375–12382.
- M. Koshimizu, K. Saeki, Y. Fujimoto, G. Okada, T. Yanagida, S. Yamashita and K. Asai, A three-state model for describing the temperature variation of the scintillation properties of  $\text{Cs}_2\text{HfCl}_6$ , *Jpn. J. Appl. Phys.*, 2018, **57**, 032401.
- M. Buryi, V. Babin, R. A. M. Ligthart, S. S. Nagorny, V. B. Mikhailik, V. Vaněček, L. P. Prochazková, R. Kandel, V. V. Nahorna and P. Wang, Correlation of emission, scintillation and charge trapping properties in  $\text{Cs}_2\text{HfCl}_6$  and  $\text{Cs}_2\text{ZrCl}_6$  single crystals, *J. Mater. Chem. C*, 2021, **9**, 2955–2968.
- K. Saeki, Y. Fujimoto, M. Koshimizu, D. Nakauchi, H. Tanaka, T. Yanagida and K. Asai, Luminescence and scintillation properties of Tl- and Ce-doped  $\text{Cs}_2\text{HfCl}_6$  crystals, *Jpn. J. Appl. Phys.*, 2017, **56**, 020307.
- Y. Fujimoto, K. Saeki, D. Nakauchi, H. Fukada, T. Yanagida, H. Kawamoto, M. Koshimizu and K. Asai, Photoluminescence, photoacoustic, and scintillation properties of Te<sup>4+</sup>-doped  $\text{Cs}_2\text{HfCl}_6$  crystals, *Mater. Res. Bull.*, 2018, **105**, 291–295.
- S. Kodama, S. Kurosawa, J. Pejchal, R. Kral, A. Yamaji, Y. Ohashi, Y. Yokota, K. Kamada, M. Nikl and A. Yoshikawa, Growth and Luminescent Properties of



- Cs<sub>2</sub>HfCl<sub>6</sub> Scintillators Doped With Alkaline Earth Metals, *IEEE Trans. Nucl. Sci.*, 2018, **65**, 2169–2173.
- 16 V. Vanecek, J. Paterek, R. Kral, M. Buryi, V. Babin, K. Zlouzeova, S. Kodama, S. Kurosawa, Y. Yokota, A. Yoshikawa and M. Nikl, Cs<sub>2</sub>HfCl<sub>6</sub> doped with Zr: Influence of tetravalent substitution on scintillation properties, *J. Cryst. Growth*, 2021, **573**, 126307.
- 17 M. Buryi, R. Kral, V. Babin, J. Paterek, V. Vanecek, P. Veverka, M. Kohoutkova, V. Laguta, M. Fasoli, I. Villa, F. Cova, A. Vedda and M. Nikl, Trapping and Recombination Centers in Cesium Hafnium Chloride Single Crystals: EPR and TSL Study, *J. Phys. Chem. C*, 2019, **123**, 19402–19411.
- 18 K. Saeki, Y. Wakai, Y. Fujimoto, M. Koshimizu, T. Yanagida, D. Nakauchi and K. Asai, Luminescence and scintillation properties of Rb<sub>2</sub>HfCl<sub>6</sub> crystals, *Jpn. J. Appl. Phys.*, 2016, **55**, 110311.
- 19 K. Saeki, Y. Fujimoto, M. Koshimizu, D. Nakauchi, H. Tanaka, T. Yanagida and K. Asai, Luminescence and scintillation properties of Cs<sub>2</sub>HfBr<sub>6</sub> and Cs<sub>2</sub>ZrBr<sub>6</sub> crystals, *Jpn. J. Appl. Phys.*, 2018, **57**, 030310.
- 20 S. Lam, C. Gugushev, A. Burger, M. Hackett and S. Motakef, Crystal growth and scintillation performance of Cs<sub>2</sub>HfCl<sub>6</sub> and Cs<sub>2</sub>HfCl<sub>4</sub>Br<sub>2</sub>, *J. Cryst. Growth*, 2018, **483**, 121–124.
- 21 P. Bhattacharya, C. Brown, C. Sosa, M. Wart, S. Miller, C. Brecher and V. V. Nagarkar, Tl<sub>2</sub>ZrCl<sub>6</sub> and Tl<sub>2</sub>HfCl<sub>6</sub> Intrinsic Scintillators for Gamma Rays and Fast Neutron Detection, *IEEE Trans. Nucl. Sci.*, 2020, **67**, 1032–1034.
- 22 R. Hawrami, E. Ariesanti, V. Buliga, L. Matei, S. Motakef and A. Burger, Advanced high-performance large diameter Cs<sub>2</sub>HfCl<sub>6</sub> (CHC) and mixed halides scintillator, *J. Cryst. Growth*, 2020, **533**, 125473.
- 23 S. Nagorny, Novel Cs<sub>2</sub>HfCl<sub>6</sub> Crystal Scintillator: Recent Progress and Perspectives, *Physics*, 2021, **3**, 320–351.
- 24 S. Maniv, Crystal Data for Cs<sub>2</sub>HfCl<sub>6</sub>, *J. Appl. Crystallogr.*, 1976, **9**, 245–245.
- 25 J. F. Ackerman, Preparation and Luminescence of Some [K<sub>2</sub>PtCl<sub>6</sub>] Materials, *Mater. Res. Bull.*, 1984, **19**, 783–791.
- 26 L. Akselrud and Y. Grin, WinCSD: software package for crystallographic calculations (Version 4), *J. Appl. Crystallogr.*, 2014, **47**, 803–805.
- 27 V. B. Mikhailik and H. Kraus, Development of techniques for characterisation of scintillation materials for cryogenic application, *Radiat. Meas.*, 2013, **49**, 7–12.
- 28 G. Engel, Die Kristallstrukturen einiger Hexachlorokomplexsalze, *Z. Kristallogr.*, 1935, **90**, 341–373.
- 29 R. Liu, W. Zhang, G. Li and W. Liu, An ultraviolet excitation anti-counterfeiting material of Sb<sup>3+</sup> doped Cs<sub>2</sub>ZrCl<sub>6</sub> vacancy-ordered double perovskite, *Inorg. Chem. Front.*, 2021, **8**, 4035–4043.
- 30 V. Brandwijk and D. L. Jongejan, The effect of pressure on A<sub>2</sub>BX<sub>6</sub> halides, contrary to the effect of pressure on ABX<sub>3</sub> halides, *Mater. Res. Bull.*, 1972, **7**, 635–639.
- 31 M. G. Brik and I. V. Kityk, Modeling of lattice constant and their relations with ionic radii and electronegativity of constituting ions of AX<sub>Y</sub> cubic crystals (A=K, Cs, Rb, Tl; X=tetravalent cation, Y=F, Cl, Br, I), *J. Phys. Chem. Solids*, 2011, **72**, 1256.
- 32 D. I. Torres, J. D. Freire and R. S. Katiyar, Lattice dynamics of crystals having R<sub>2</sub>MX<sub>6</sub> structure, *Phys. Rev. B: Condens. Matter Mater. Phys.*, 1997, **56**, 7763–7766.
- 33 A. Senyshyn, H. Kraus, V. B. Mikhailik and V. Yakovyna, Lattice dynamics and thermal properties of CaWO<sub>4</sub>, *Phys. Rev. B: Condens. Matter Mater. Phys.*, 2004, **70**, 214306.
- 34 C. Cardenas, A. Burger, B. Goodwin, M. Groza, M. Laubenstein, S. Nagorny and E. Rowe, Pulse-shape discrimination with Cs<sub>2</sub>HfCl<sub>6</sub> crystal scintillator, *Nucl. Instrum. Methods Phys. Res., Sect. A*, 2017, **869**, 63–67.
- 35 V. Alenkov, O. A. Buzanov, N. Khanbekov, V. N. Kornoukhov, H. Kraus, V. B. Mikhailik and V. A. Shuvaeva, Application of the Monte-Carlo refractive index matching (MCRIM) technique to the determination of the absolute light yield of a calcium molybdate scintillator, *J. Instrum.*, 2013, **8**, P06002.
- 36 V. B. Mikhailik and H. Kraus, Scintillators for cryogenic applications: State-of-art, *J. Phys. Stud.*, 2010, **14**, 4201.
- 37 H. Shibata, Negative thermal quenching curves in photoluminescence of solids, *Jpn. J. Appl. Phys.*, 1998, **37**, 550–553.
- 38 S. Lam, M. Gascon, R. Hawrami, W. Setyawan, S. Curtarolo, R. S. Feigelson and R. M. Gaume, Nonproportionality and Scintillation Studies of Eu:SrI<sub>2</sub> From 295 to 5 K, *IEEE Trans. Nucl. Sci.*, 2012, **59**, 2052–2056.
- 39 L. Swiderski, K. Brylew, W. Drozdowski, M. Grodzicka-Kobylka, L. Janiak and M. Moszynski, LuAG:Pr, LuAG:Pr, Mo and LuYAG:Pr relative light yield measured at wide temperature range with MPPC readout, *Nucl. Instrum. Methods Phys. Res., Sect. A*, 2022, **1021**, 165924.

